JOINT EUROPEAN TORUS JET

JET–P(90)65

L.A. Charlton, L.R. Baylor, A. Edwards, G.W. Hammett, W.A. Houlberg,
P. Kupschus, V.E. Lynch, S.L. Miloral, J. O'Rourke, G.L. Schmidt
and JET Team

MHD Analysis of Peaked Pressure Profiles Produced by Pellet Injection in JET

MHD Analysis of Peaked Pressure Profiles Produced by Pellet Injection in JET

L.A. Charlton[1], L.R. Baylor[1], A. Edwards, G.W. Hammett, W.A. Houlberg[1], P. Kupschus, V.E. Lynch[1], S.L. Miloral, J. O'Rourke, G.L. Schmidt[2] and JET Team*

JET-Joint Undertaking, Culham Science Centre, OX14 3DB, Abingdon, UK

1 Oak Ridge National Laboratory, Oak Ridge, Tennessee, USA.
2 Princeton Plasma Physics Laboratory, Princeton, New Jersey, USA.

** See Appendix 1*

Preprint of Paper to be submitted for publication in
Nuclear Fusion

ABSTRACT.

The cery peaked pressure profiles in some pellet-fueled discharges with ion cyclotron resonance heating (ICRH) in the Joint European Torus (JET) are terminated by an abrupt flattening oi the temperature profile. This appears to be the result of an instability with a very fast time scale that is triggered when the safety factor q drops below 1.5. The ideal m/n = 3/2 infernal mode, which is excited only when q is very close to 1.5; may well be the responsible instability. Linear magnetohydrodynamic (MHD) stability calculations, based on equilibria that model the relevant JET discharges as closely as possible, yield growth rates consistent with the rise time of the instability. Nonlinear calculations initialized with the same equilibria exhibit plasma behavior very similar to that seen experimentally: (1) a flattening of the pressure profile occurs, (2) a residual m = 3 structure is present after the flattening, and (3) the time scale for the flattening is in reasonable agreement with experimental observations. It is thus concluded that the ideal infernal mode is an excellent candidate for the instability.

1. INTRODUCTION

In some pellet-fueled discharges with ion cyclotron resonance heating (ICRH) in the Joint European Torus (JET), an instability with a very fast time scale instability causes an abrupt flattening of the central electron and ion temperatures [1]. The time dependence of various plasma parameters during one such discharge (discharge 16211) is shown in Fig. 1, with results from the predictive transport code WHIST (up to the time of the collapse) [2] shown for comparison. During the first 1.3 s of heating with 6 to 8 MW of ICRH power following injection of a 4.0 mm diam, 4.0 mm long cylindrical pellet at 3.0 s, the elevated core density decays gradually inside $\rho/a < 0.6$. The peaked portion of the density profile is superimposed on a very broad baseline density profile. During this phase, the central electron and ion temperatures increase rapidly (up to 12 keV and 10 keV, respectively, in the best discharges). This results in an increase in the central plasma pressure by approximately a factor of three ($\beta(0) = 5\%$) above that seen in gas-fueled discharges and gives rise to sharply increased pressure gradients in the plasma core. There appears to be no degradation of confinement in the core during the first 1.3 s of auxiliary heating; in fact, transport analysis shows that both particle and thermal diffusivities are strongly suppressed in the core [3]. As shown in Fig. 1, an abrupt collapse of the central electron and ion temperatures terminates the enhanced confinement phase at 4.3 s and leads eventually to a 20% decrease in plasma stored energy. Note that the central safety factor q_0 reaches a value of 1.5 at about the time of the termination of the enhanced confinement phase.

We examine two discharges that showed this behavior: discharge 16211 (described above), which we label A, and discharge 17749, which we label B. Discharge B had a large, abrupt increase in $n = 2$ magnetohydrodynamic (MHD) activity at the time of the instability (a larger increase than for any other n). In one discharge (discharge 17689) similar to discharges A and B, there was an $m = 3$ successor after the collapse. It is thus assumed that the instability is $m/n = 3/2$. By looking at the rise time of the MHD

signals for discharge 17689, we can estimate the inverse growth rate for the responsible mode to be $\gamma^{-1} \leq 100\,\mu$s. Using the plasma parameters of discharge A, we find that the poloidal Alfvén time $\tau_{\rm Hp} \approx 0.3\,\mu$s ($\tau_{\rm Hp} \propto R\sqrt{n}/B_T$, $R = 3.0$ m, $n = 0.6 \times 10^{20}$ m^{-3}, and $B_T = 3$ T). Thus, the dimensionless growth rate is $\gamma\tau_{\rm Hp} = 0.003$. The resistive time for the same discharge is $\tau_{\rm R} \approx 4.3 \times 10^3$ s ($\tau_{\rm R} \propto T^{3/2}a^2$, $T = 12$ keV, $a = 1.2$ m). The magnetic Reynolds number is large, $S = \tau_{\rm R}/\tau_{\rm Hp} \approx 10^{10}$, and a resistive mode should have rather slow growth. Because of these conditions, we consider only ideal $n = 2$ modes in this study.

Unless stated otherwise, all equilibria that we discuss are ballooning ($n = \infty$) stable. The toroidal geometry, nonlinear, resistive MHD code FAR [4] is used in our analysis, with all results tested for convergence. In Section 2 the equilibria and the linear growth rates are given. Nonlinear results are presented in Section 3.

2. EQUILIBRIA AND LINEAR RESULTS

The collapse of the central temperature in discharge A was studied by parameterizing the pressure p and q profiles taken from the time-dependent transport analysis code TRANSP [3]. The TRANSP profiles are those just before the temperature collapse when $q_0 \approx 1.5$. The parameterized profiles and those from TRANSP are compared in Fig. 2. The difference between the two is regarded as negligible. Small differences near the axis result from the slightly hollow nature of the experimental current profile, which is due to the bootstrap current as calculated by TRANSP. The inclusion of appreciable bootstrap current could stabilize these modes near the magnetic axis by introducing shear. These profiles, together with the parameters shown in Table I for discharge A, give an equilibrium that is unstable to an $m/n = 3/2$ infernal mode [5] with a growth rate of $\gamma\tau_{\mathrm{Hp}} = 0.0053$. This value is consistent with the estimate discussed in Section 1.

Figure 3 shows a variety of pressure profiles, including that given by TRANSP for a q profile identical to that in Fig. 2. These pressure profiles were chosen to give a wide range of pressure gradients in the plasma interior while maintaining a constant central pressure. Equilibria were generated for each of these profiles. All are infernal mode unstable with growth rates varying from 0.0050 to 0.0107; within a factor of three of the estimated experimental value.

Discharge B was analyzed first by using an equilibrium from the IDENTC code [6], which gives equilibria that match a variety of experimental parameters. The pressure profile was much wider than those shown in Figs 2 and 3 for discharge A, and the equilibrium was $n = 2$ stable but ballooning ($n = \infty$) unstable.

Data from the LIDAR system [7] indicated that the pressure profiles for these discharges just before the temperature flattening were much narrower than those used in the initial IDENTC calculations. Thus, the pressure profiles used to generate equilibria for the study of discharge B were taken to bracket the profile in Ref. [7], as shown in Fig. 4. The

pressure profiles are plotted as a function of the distance from the magnetic axis outboard along the midplane (normalized to unity at the plasma edge). The q profile was identical to that used for shot A (shown in Fig. 2(b)). Other plasma parameters used are shown in Table I. All equilibria for discharge B using these pressure profiles are infernal mode unstable with growth rates somewhat smaller than those for discharge A.

There are two significant differences between the two sets of equilibria: those for discharge A have both higher β, which is destabilizing, and larger elongation, which is stabilizing. Thus, the effect of higher β is dominant in these calculations, since the growth rates for discharge A are about a factor of two larger than those for discharge B.

Figure 5 shows the instability velocity vectors at various points in the plasma for the equilibrium with $\gamma\tau_{\mathrm{Hp}} = 0.0053$ discussed at the beginning of this section. This behavior is typical of infernal mode instabilities. The length of the vectors can be taken as a measure of the activity at any point. Thus, regions with longer vectors appear darker and are regions of greatest instability. There is also some indication of instability near rational surfaces away from the center of the plasma. However, the relevant instability in the cases that we are examining here is in the center of the plasma, where the temperature flattening takes place. Thus, these equilibria are unstable in a manner that is suggestive of the observed behavior.

Perhaps the most dramatic signature of infernal modes is the sudden onset of instability as q_0 (safety factor at the magnetic axis) passes through low-order rational values. The linear growth rate as a function of q_0 in the vicinity of $q_0 = 3/2$ is shown in Fig. 6 for the initial equilibrium used for shot A (Fig. 2 and Table I) and for one of the equilibria studied for shot B.

3. NONLINEAR RESULTS

To evaluate the influence of the instability on the pressure profile, we use the FAR code [4] to follow the nonlinear evolution of one of the toroidal geometry equilibria for discharge A and compare it with the nonlinear evolution of a similar cylindrical geometry equilibrium. Since a maximum value of $S = 1 \times 10^5$ is required for numerical reasons, the resistivity used for the nonlinear studies is larger than the experimental resistivity (corresponding to $S \approx 10^{10}$). The calculated evolution of the ideal infernal mode described here, however, is not expected to be much different from that for larger values of S; the linear growth rate of this ideal mode is, of course, independent of the value of S.

The lesser strength of the instability in toroidal geometry is clear in Fig. 7, where the peak value of the plasma pressure is plotted versus time. The toroidal case is the one whose linear stability was discussed earlier for discharge A (linear growth rate $\gamma\tau_{HP} = 0.0107$ identified in Fig. 3), and the cylindrical geometry case has an aspect ratio of 4.0. The peak pressure in the toroidal case starts decreasing later, has a longer time scale for saturation, and decreases by about half the amount calculated for the cylindrical case. The gross behavior is, however, qualitatively the same for both cases. Comparison with Fig. 1 shows that the drop in central pressure is consistent with the experimental data.

The characteristics of the pressure profile evolution can be seen in Fig. 8. An $m = 3$ structure appears, the central pressure decreases, and the profile broadens. After saturation the temperature is essentially flat, but some $m = 3$ structure is still evident. This $m = 3$ structure is seen in the JET soft X-ray emissivity profiles after the temperature collapses [1]. The pressure profile evolution for the toroidal case is very similar to that for the cylindrical case. Constant-pressure contours in the core region for the toroidal case are shown in Fig. 9. Again, an $m = 3$ structure is very strong while the central pressure is decreasing, and the characteristic triangular $m = 3$ shape persists after saturation of the central pressure drop.

Field line plots from the evolution of the toroidal case show the time dependence of the magnetic structure in Fig. 10. These puncture plots were generated by following a field line many times around the torus and recording a point whenever the field line passed through a given toroidal angle. These plots are in real-space coordinates (in contrast to the previous two figures), and the elongated shape of the plasma can be seen. At the earliest times, concentric flux surfaces are apparent. Later, the $m = 3$ structure appears in the magnetic surfaces; then a substantial amount of ergodicity develops. The degree of ergodicity depends on the resistivity, and, as discussed earlier, the resistivity used was larger than the experimental value. The degree of ergodicity shown here is therefore of limited relevance for the JET discharges considered. It is noted experimentally, however, that confinement in the core is degraded for the remainder of the heating pulse (L-mode), since the central temperatures never recover.

4. SUMMARY

The very peaked pressure profiles following pellet injection and central ICRH in the early portion of JET discharges have consistently exhibited evidence of an MHD instability that results in a flattening of the central temperature. These data provide a significant test for MHD stability analyses. We conclude that the infernal mode is a strong candidate for the instability in the discharges considered. This instability is associated with the appearance of $q = 3/2$ in the plasma core as the central current increases early in the discharge. Equilibria calculated with experimental pressure profiles and $q_0 < 1.5$ show instability growth rates that agree with experimental observations. Because of uncertainties in matching experimental data, several equilibria have been examined for each case; all are infernal mode unstable. Nonlinear analysis shows a strong $m = 3$ structure during the temperature flattening and a persistence of the structure after the temperature flattening. This structure is observed in soft X-ray data.

REFERENCES

[1] SCHMIDT, G. L., JET TEAM, in Plasma Physics and Controlled Nuclear Fusion Research 1988 (Proc. 12th Int. Conf. Nice, 1988), Vol. 1, IAEA, Vienna (1989) 215.

[2] HOULBERG, W. A., MILORA, S. L., PHILLIPS, C. K., TOLLIVER, J. S., JET/US PELLET TEAM, in Pellet Injection and Toroidal Confinement, (Proc. Tech. Committee Meeting, Gut Ising, 1988), IAEA-TECDOC-534, IAEA, Vienna (1989) 137.

[3] HAMMETT, G., COLESTOCK, P. L., GRANETZ, R. S., KUPSCHUS, P., McCUNE, D. C., PHILLIPS, C. K., SCHMIDT, G. L., SMITHE, D. N., JET/US PELLET TEAM, in Controlled Fusion and Plasma Physics (Proc. 16th Eur. Conf. Venice, 1989). Vol. 13B, Part I, European Physical Society (1989) 131.

[4] CHARLTON, L. A., CARRERAS, B. A., HOLMES, J. A., LYNCH, V. E., HENDER, T. C., J. Comput. Phys. **86** (1990) 270.

[5] MANICKAM, J., POMPHREY, N., TODD, A. M. M., Nucl. Fusion **27** (1987) 1461: CHARLTON, L. A., HASTIE, R. J., HENDER, T. C., Phys. Fluids B **1** (1989) 798: CHARLTON, L. A., CARRERAS, B. A., LYNCH, V. E., Phys. Fluids B **2** (1990) 1574.

[6] LAZZARO, E., MANTICA, P., Plasma Phys. Controlled Fusion **30** (1988) 1735.

[7] GALVÃO, R. M. O., GOEDBLOED, J. P., HUYSMANS, G., LAZZARO, E., O'ROURKE, J., SCHMIDT, G., SMEULDERS, P., in Controlled Fusion and Plasma Physics (Proc. 16th Eur. Conf. Venice, 1989), Vol. 13B, Part II, European Physical Society (1989) 501.

TABLE I. JET PARAMETERS FOR MODELLED DISCHARGES

Discharge	β_0 (%)	Elongation κ	Central safety factor q_0	Edge safety factor q_a
A	5.0	1.47	1.5	4.8
B	4.4	1.33	1.5	4.1

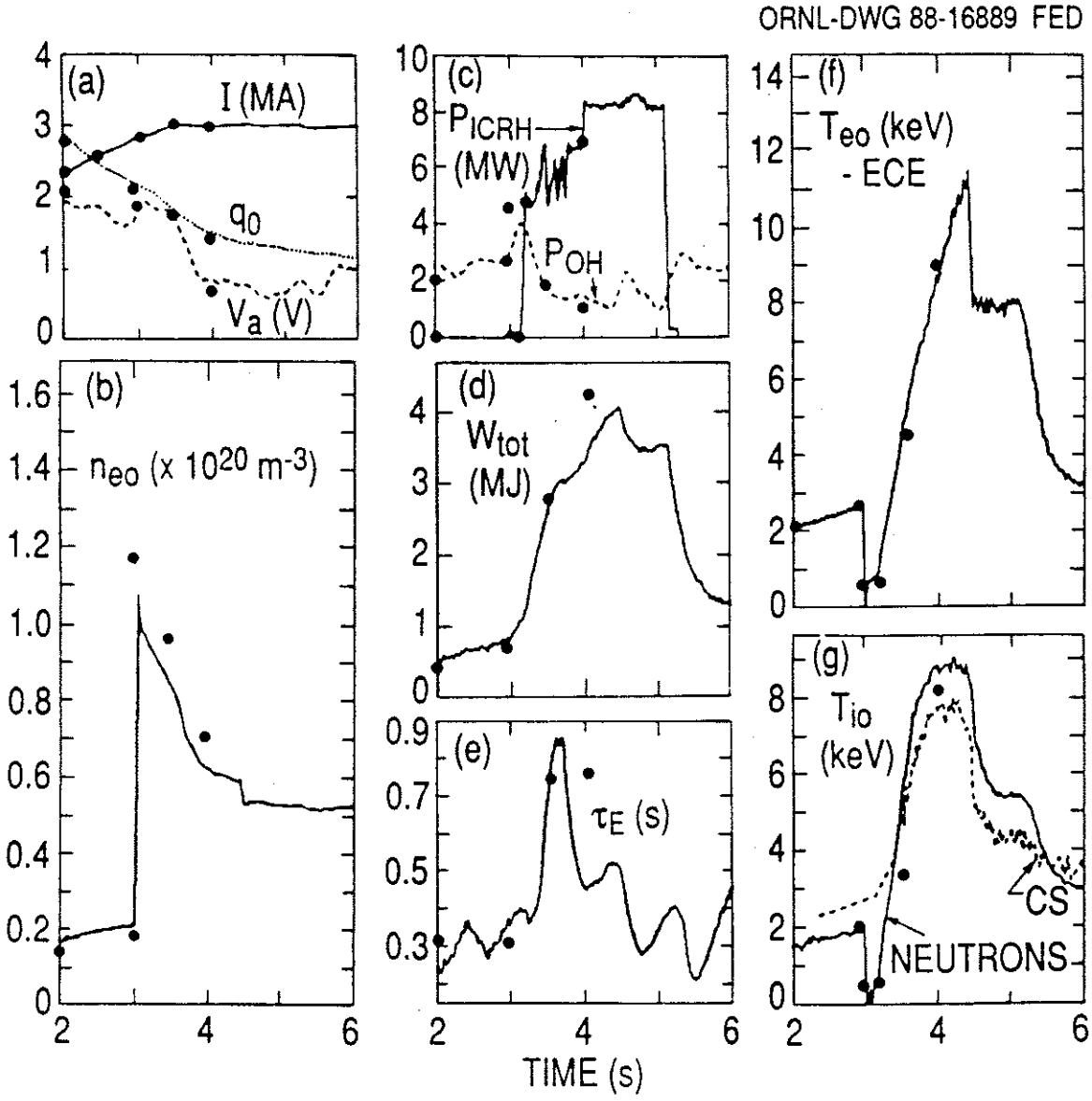

FIG. 1. Summary of the time dependence of various plasma parameters for JET discharge 16211: (a) toroidal current I, central safety factor q_0, and toroidal loop voltage V_a; (b) central electron density n_{e0}; (c) ICRH and Ohmic heating power, $P_{\rm ICRH}$ and $P_{\rm OH}$; (d) total kinetic energy $W_{\rm tot}$; (e) global energy confinement time τ_E; (f) central electron temperature T_{e0}; and (g) central ion temperature T_{i0}. The points are results from predictive simulation of the early portion of the discharge using the WHIST code.

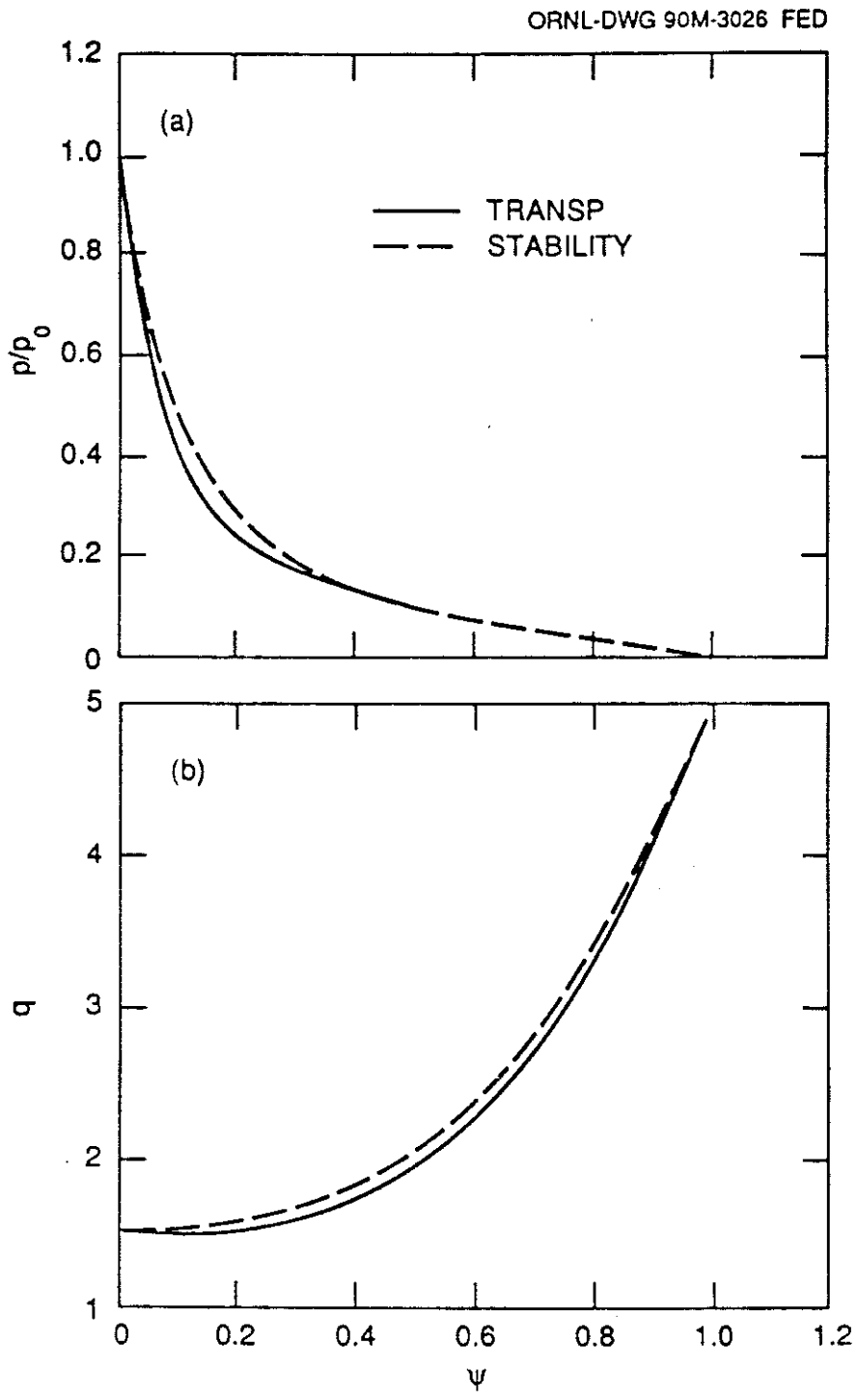

FIG. 2. Normalized (a) pressure and (b) safety factor profiles from the TRANSP analysis code and those used for the initial stability study of discharge A. The minor radial coordinate is represented by the dimensionless poloidal flux ψ.

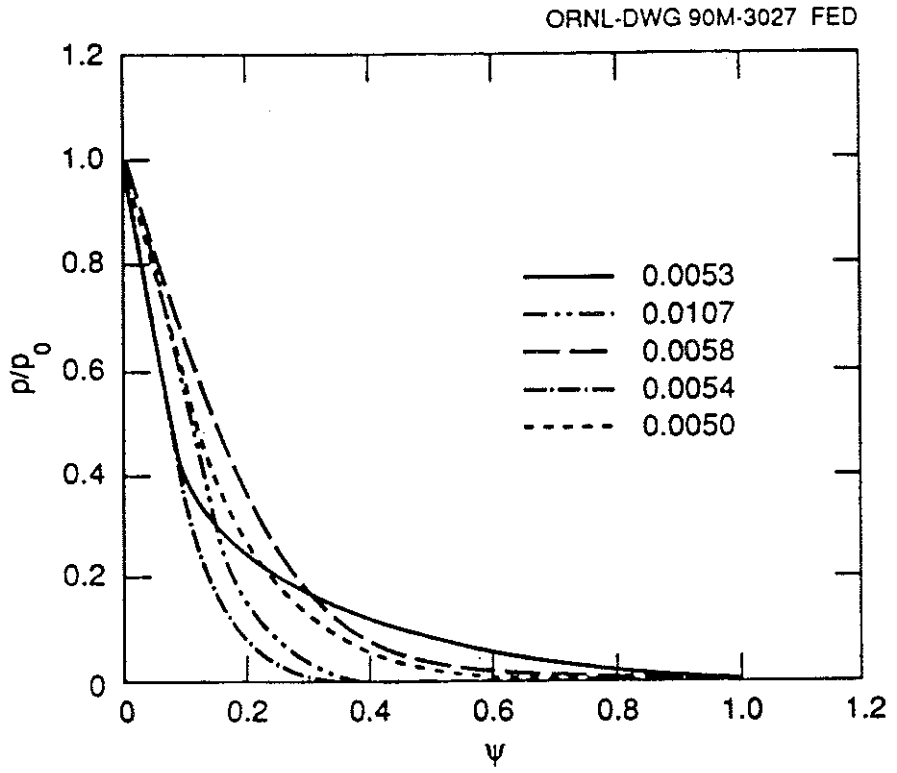

FIG. 3. Pressure profiles used to test the sensitivity of the results to profile changes. Each profile is labelled by the resulting linear growth rate for an $m/n = 3/2$ infernal mode in units of τ_{Hp}^{-1}. The q profile used is identical to that in Fig. 2(b) in all cases. The pressure profile from TRANSP is labeled 0.0053.

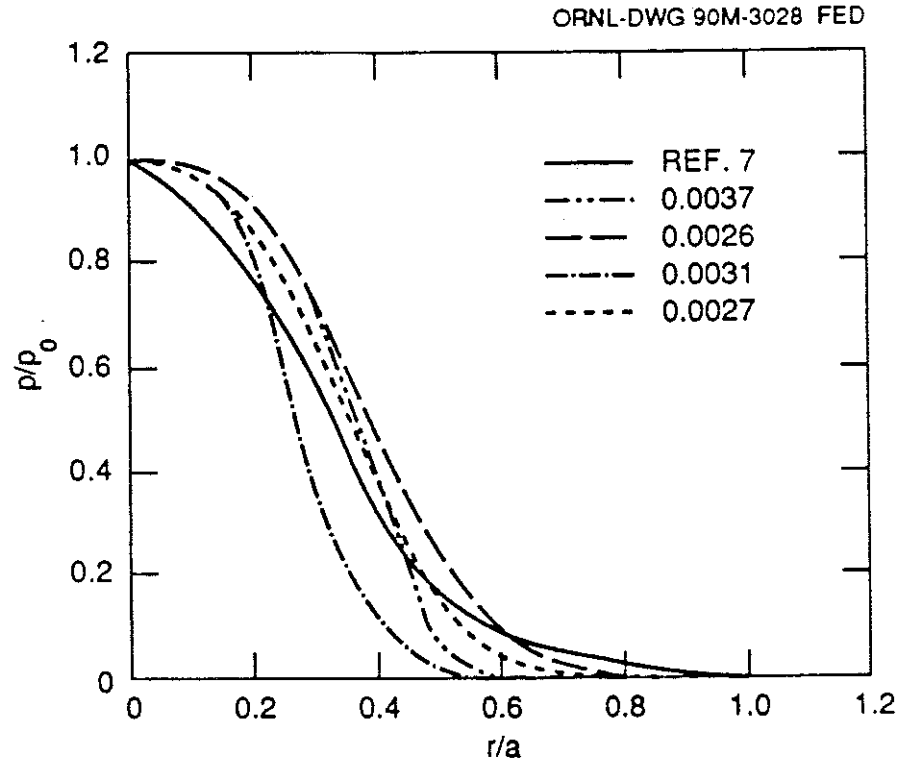

FIG. 4. Pressure profiles used for the stability study of discharge B and the experimental profile from Ref. [7]. Each profile is labeled by the linear growth rate in units of τ_{Hp}^{-1}.

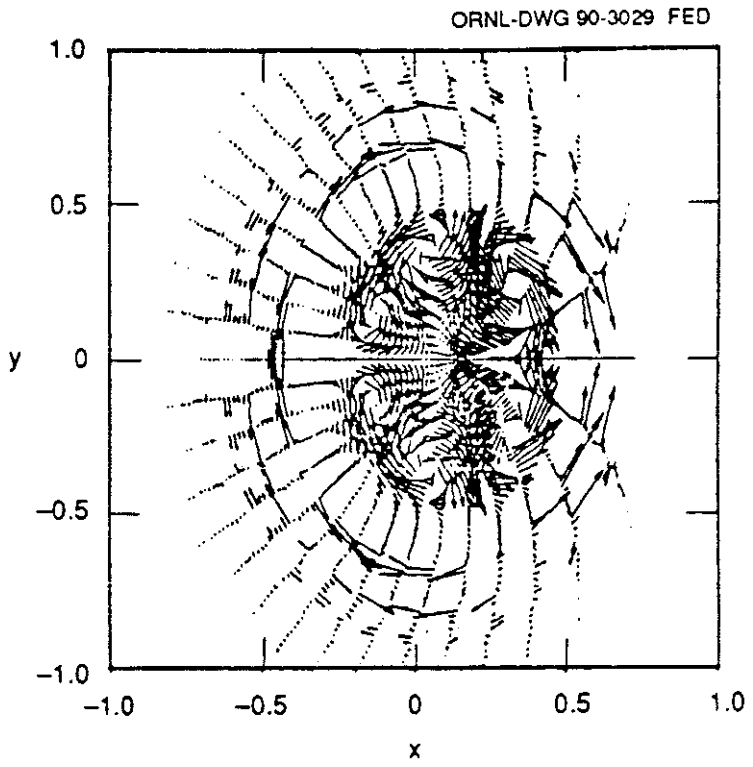

FIG. 5. Instability velocity vectors. The length of the vectors is a measure of the strength of the instability.

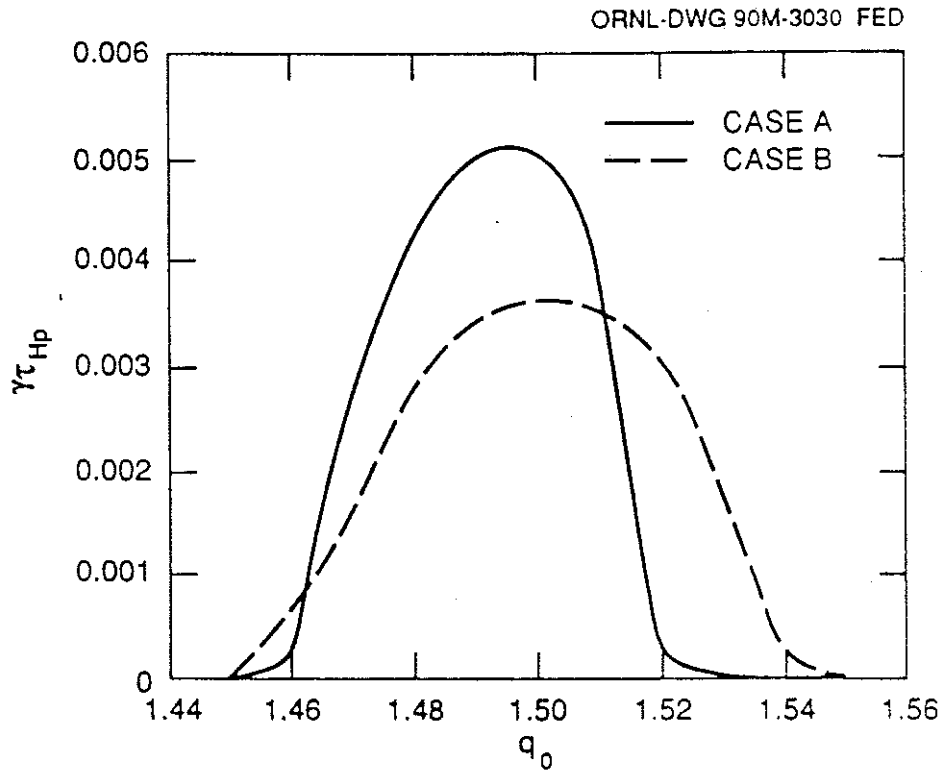

FIG. 6. The growth rate of the instability ($\gamma\tau_{Hp}$) is localized to a small band around $q_0 = 1.5$ in both case A (16211) and case B (17749).

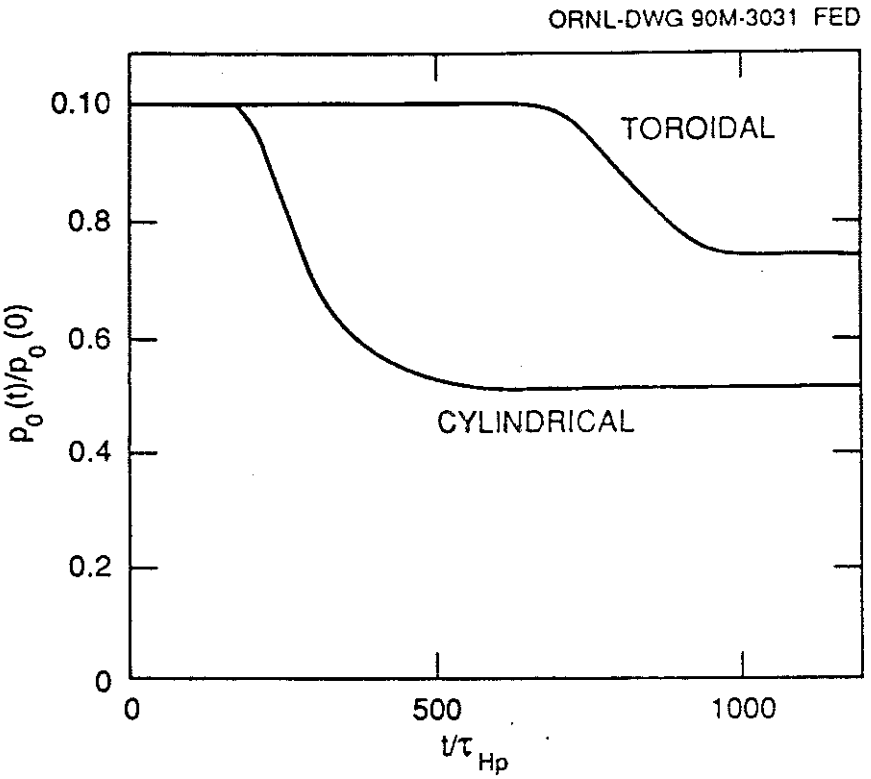

FIG. 7. The peak pressure (normalized to unity at $t = 0$) decreases somewhat more slowly and saturates with a smaller drop in the toroidal case than in the cylindrical case.

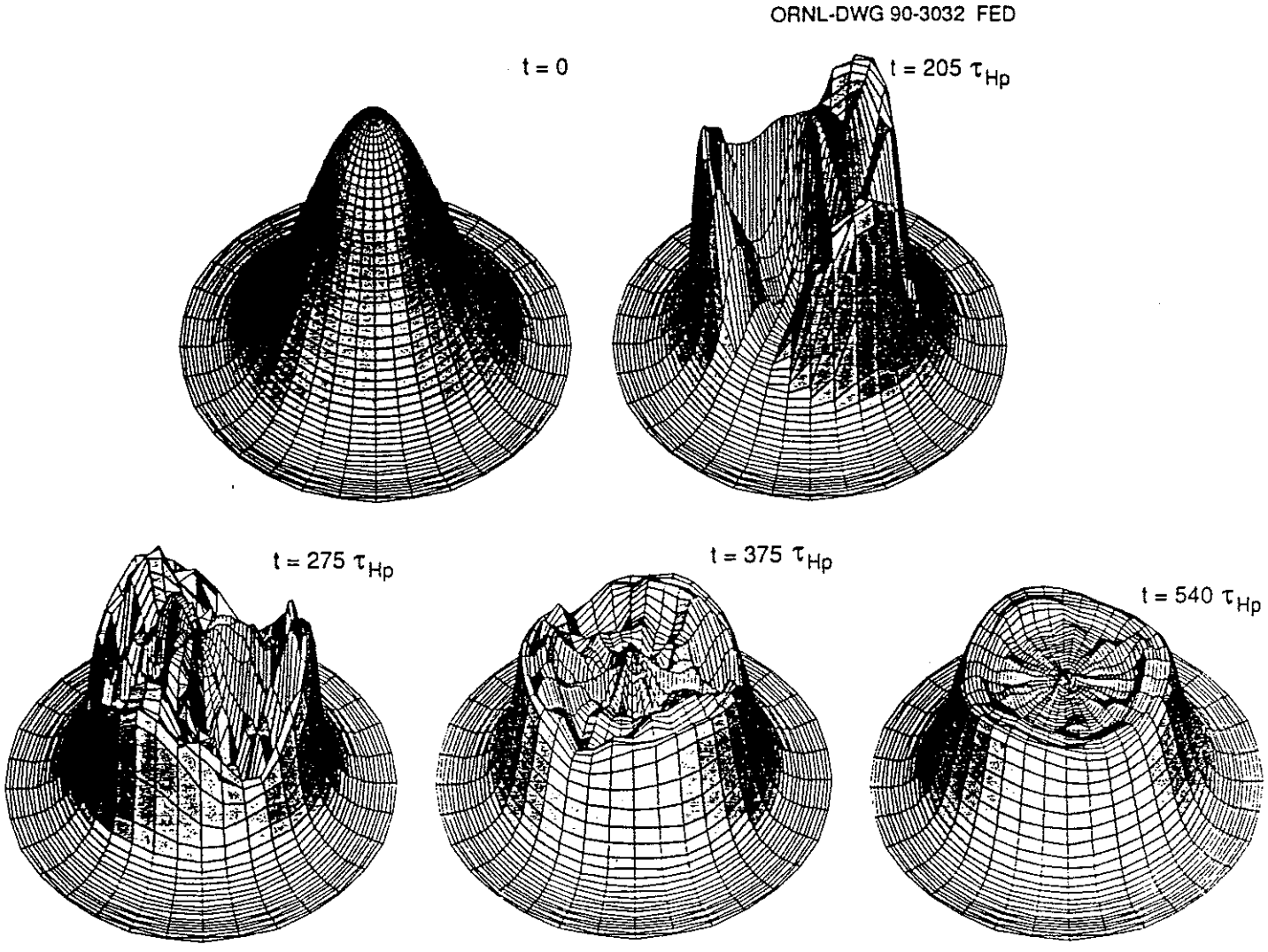

FIG. 8. Pressure contours during the nonlinear evolution of the circular, cylindrical equilibrium, showing the $m = 3$ structure.

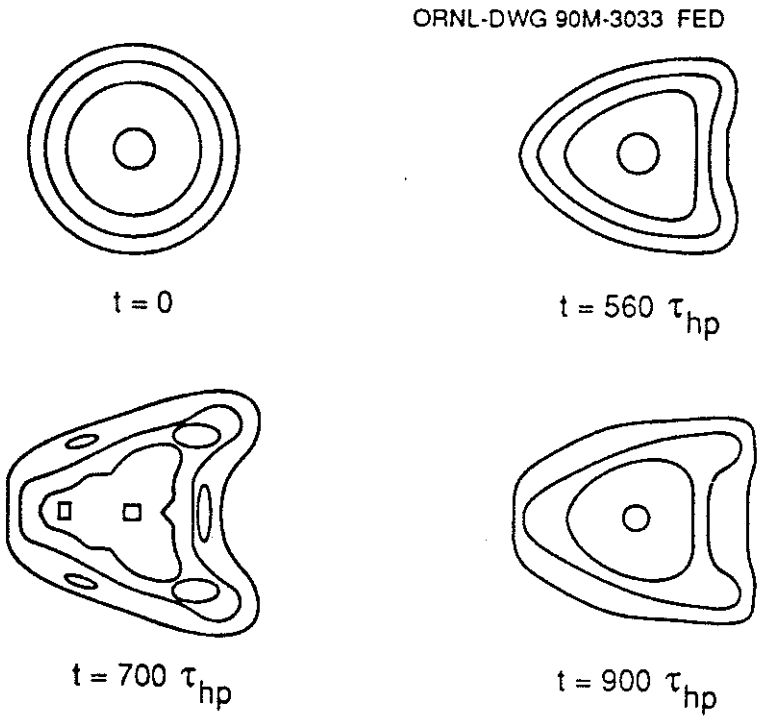

FIG. 9. Pressure contours in (ψ, θ) space during the nonlinear evolution of the toroidal equilibrium also show $m = 3$ structure. Only contours in the plasma interior are shown. The contours would be vertically elongated in real space.

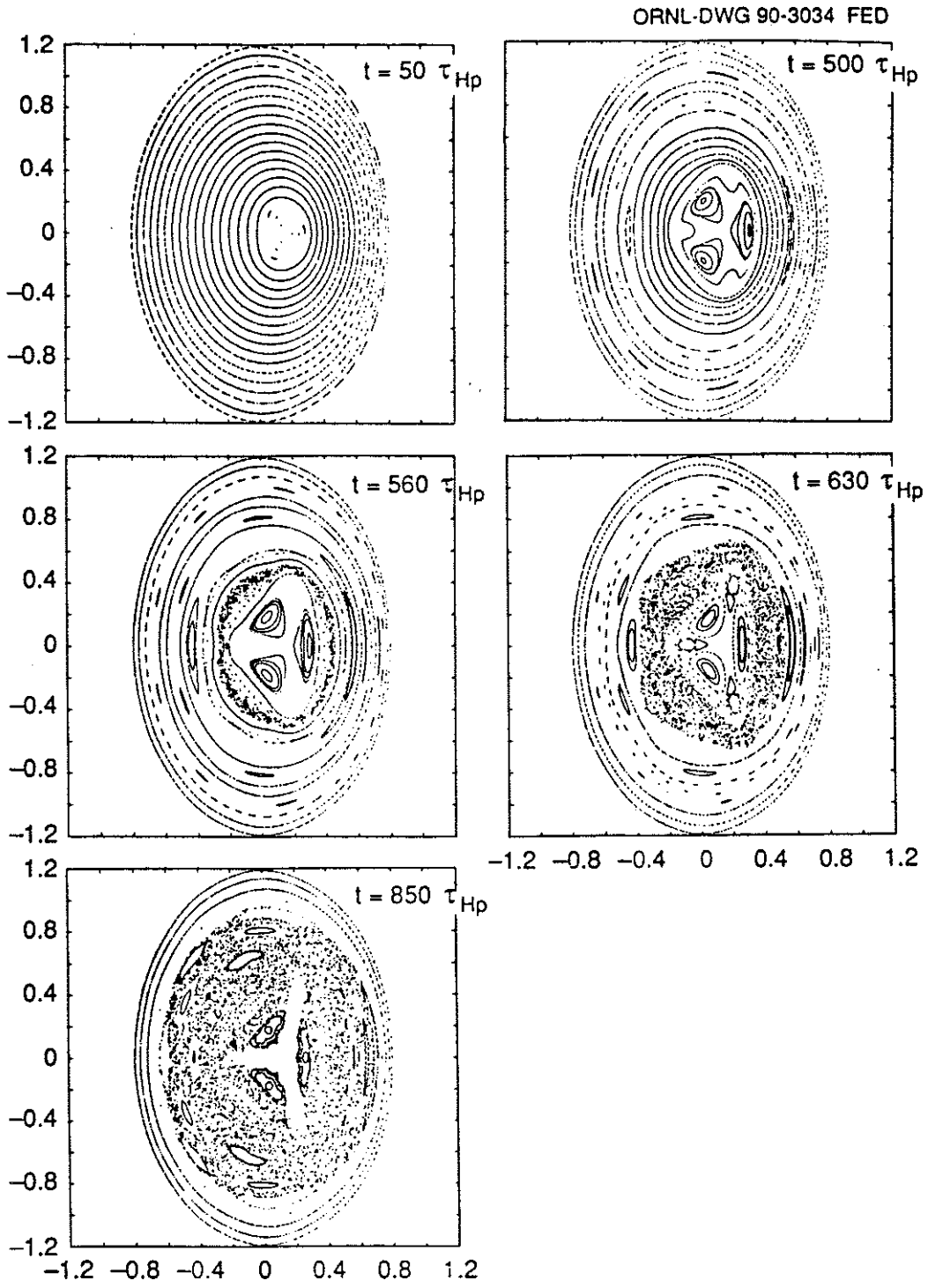

FIG. 10. Field line plots at various times during the nonlinear evolution of the toroidal equilibrium, showing development of an $m = 3$ structure followed by a large region of ergodicity in the core.

APPENDIX 1.

THE JET TEAM

JET Joint Undertaking, Abingdon, Oxon, OX14 3EA, U.K.

J.M.Adams[1], F.Alladio[4], H.Altmann, R.J.Anderson, G.Appruzzese, W.Bailey, B.Balet, D.V.Bartlett, L.R.Baylor[24], K.Behringer, A.C.Bell, P.Bertoldi, E.Bertolini, V.Bhatnagar, R.J.Bickerton, A.Boileau[3], T.Bonicelli, S.J.Booth, G.Bosia, M.Botman, D.Boyd[31], H.Brelen, H.Brinkschulte, M.Brusati, T.Budd, M.Bures, T.Businaro[4], H.Buttgereit, D.Cacaut, C.Caldwell-Nichols, D.J.Campbell, P.Card, J.Carwardine, G.Celentano, P.Chabert[27], C.D.Challis, A.Cheetham, J.Christiansen, C.Christodoulopoulos, P.Chuilon, R.Claesen, S.Clement[30], J.P.Coad, P.Colestock[6], S.Conroy[13], M.Cooke, S.Cooper, J.G.Cordey, W.Core, S.Corti, A.E.Costley, G.Cottrell, M.Cox[7], P.Cripwell[13], F.Crisanti[4], D.Cross, H.de Blank[16], J.de Haas[16], L.de Kock, E.Deksnis, G.B.Denne, G.Deschamps, G.Devillars, K.J.Dietz, J.Dobbing, S.E.Dorling, P.G.Doyle, D.F.Düchs, H.Duquenoy, A.Edwards, J.Ehrenberg[14], T.Elevant[12], W.Engelhardt, S.K.Erents[7], L.G.Eriksonn[5], M.Evrard[2], H.Falter, D.Flory, M.Forrest[7], C.Froger, K.Fullard, M.Gadeberg[11], A.Galetsas, R.Galvao[8], A.Gibson, R.D.Gill, A.Gondhalekar, C.Gordon, G.Gorini, C.Gormezano, N.A.Gottardi, C.Gowers, B.J.Green, F.S.Griph, M.Gryzinski[26], R.Haange, G.Hammett[6], W.Han[9], C.J.Hancock, P.J.Harbour, N.C.Hawkes[7], P.Haynes[7], T.Hellsten, J.L.Hemmerich, R.Hemsworth, R.F.Herzog, K.Hirsch[14], J.Hoekzema, W.A.Houlberg[24], J.How, M.Huart, A.Hubbard, T.P.Hughes[32], M.Hugon, M.Huguet, J.Jacquinot, O.N.Jarvis, T.C.Jernigan[24], E.Joffrin, E.M.Jones, L.P.D.F.Jones, T.T.C.Jones, J.Källne, A.Kaye, B.E.Keen, M.Keilhacker, G.J.Kelly, A.Khare[15], S.Knowlton, A.Konstantellos, M.Kovanen[21], P.Kupschus, P.Lallia, J.R.Last, L.Lauro-Taroni, M.Laux[33], K.Lawson[7], E.Lazzaro, M.Lennholm, X.Litaudon, P.Lomas, M.Lorentz-Gottardi[2], C.Lowry, G.Magyar, D.Maisonnier, M.Malacarne, V.Marchese, P.Massmann, L.McCarthy[28], G.McCracken[7], P.Mendonca, P.Meriguet, P.Micozzi[4], S.F.Mills, P.Millward, S.L.Milora[24], A.Moissonnier, P.L.Mondino, D.Moreau[17], P.Morgan, H.Morsi[14], G.Murphy, M.F.Nave, M.Newman, L.Nickesson, P.Nielsen, P.Noll, W.Obert, D.O'Brien, J.O'Rourke, M.G.Pacco-Düchs, M.Pain, S.Papastergiou, D.Pasini[20], M.Paume[27], N.Peacock[7], D.Pearson[13], F.Pegoraro, M.Pick, S.Pitcher[7], J.Plancoulaine, J-P.Poffé, F.Porcelli, R.Prentice, T.Raimondi, J.Ramette[17], J.M.Rax[27], C.Raymond, P-H.Rebut, J.Removille, F.Rimini, D.Robinson[7], A.Rolfe, R.T.Ross, L.Rossi, G.Rupprecht[14], R.Rushton, P.Rutter, H.C.Sack, G.Sadler, N.Salmon[13], H.Salzmann[14], A.Santagiustina, D.Schissel[25], P.H.Schild, M.Schmid, G.Schmidt[6], R.L.Shaw, A.Sibley, R.Simonini, J.Sips[16], P.Smeulders, J.Snipes, S.Sommers, L.Sonnerup, K.Sonnenberg, M.Stamp, P.Stangeby[19], D.Start, C.A.Steed, D.Stork, P.E.Stott, T.E.Stringer, D.Stubberfield, T.Sugie[18], D.Summers, H.Summers[20], J.Taboda-Duarte[22], J.Tagle[30], H.Tamnen, A.Tanga, A.Taroni, C.Tebaldi[23], A.Tesini, P.R.Thomas, E.Thompson, K.Thomsen[11], P.Trevalion, M.Tschudin, B.Tubbing, K.Uchino[29], E.Usselmann, H.van der Beken, M.von Hellermann, T.Wade, C.Walker, B.A.Wallander, M.Walravens, K.Walter, D.Ward, M.L.Watkins, J.Wesson, D.H.Wheeler, J.Wilks, U.Willen[12], D.Wilson, T.Winkel, C.Woodward, M.Wykes, I.D.Young, L.Zannelli, M.Zarnstorff[6], D.Zasche[14], J.W.Zwart.

PERMANENT ADDRESS

1. UKAEA, Harwell, Oxon. UK.
2. EUR-EB Association, LPP-ERM/KMS, B-1040 Brussels, Belgium.
3. Institute National des Récherches Scientifique, Quebec, Canada.
4. ENEA-CENTRO Di Frascati, I-00044 Frascati, Roma, Italy.
5. Chalmers University of Technology, Göteborg, Sweden.
6. Princeton Plasma Physics Laboratory, New Jersey, USA.
7. UKAEA Culham Laboratory, Abingdon, Oxon. UK.
8. Plasma Physics Laboratory, Space Research Institute, Sao José dos Campos, Brazil.
9. Institute of Mathematics, University of Oxford, UK.
10. CRPP/EPFL, 21 Avenue des Bains, CH-1007 Lausanne, Switzerland.
11. Risø National Laboratory, DK-4000 Roskilde, Denmark.
12. Swedish Energy Research Commission, S-10072 Stockholm, Sweden.
13. Imperial College of Science and Technology, University of London, UK.
14. Max Planck Institut für Plasmaphysik, D-8046 Garching bei München, FRG.
15. Institute for Plasma Research, Gandhinagar Bhat Gujat, India.
16. FOM Instituut voor Plasmafysica, 3430 Be Nieuwegein, The Netherlands.
17. Commissiariat à L'Energie Atomique, F-92260 Fontenay-aux-Roses, France.
18. JAERI, Tokai Research Establishment, Tokai-Mura, Naka-Gun, Japan.
19. Institute for Aerospace Studies, University of Toronto, Downsview, Ontario, Canada.
20. University of Strathclyde, Glasgow, G4 ONG, U.K.
21. Nuclear Engineering Laboratory, Lapeenranta University, Finland.
22. JNICT, Lisboa, Portugal.
23. Department of Mathematics, Univeristy of Bologna, Italy.
24. Oak Ridge National Laboratory, Oak Ridge, Tenn., USA.
25. G.A. Technologies, San Diego, California, USA.
26. Institute for Nuclear Studies, Swierk, Poland.
27. Commissiariat à l'Energie Atomique, Cadarache, France.
28. School of Physical Sciences, Flinders University of South Australia, South Australia SO42.
29. Kyushi University, Kasagu Fukuoka, Japan.
30. Centro de Investigaciones Energeticas Medioambientales y Techalogicas, Spain.
31. University of Maryland, College Park, Maryland, USA.
32. University of Essex, Colchester, UK.
33. Akademie de Wissenschaften, Berlin, DDR.

CR 88.49.1A